Comparison of Results from Recent NNSA and CEA Measurements of the ^{239}Pu(n, f) Prompt Fission Neutron Spectrum

K.J. J Kelly, Paola Marini, J. Taieb, M. Devlin, D. Neudecker, R.C. C Haight, G. Bélier, B. Laurent, P. Morfouace, J.M. M O'Donnell, et al.

Comparison of Results from Recent NNSA and CEA Measurements of the ^{239}Pu(n,f) Prompt Fission Neutron Spectrum

K. J. Kelly[1], P. Marini[2,3], J. Taieb[2,4], M. Devlin[1], D. Neudecker[1], R. C. Haight[1], G. Bélier[2,4], B. Laurent[2,4], P. Morfouace[2,4], J. M. O'Donnell[1], E. Bauge[2,4], M. B. Chadwick[1], A. Chatillon[2,4], D. Etasse[5], P. Talou[1], M. C. White[1], C. Y. Wu[6], and E. A. Bennett[1]

[1]Los Alamos National Laboratory, Los Alamos, New Mexico 87545, USA
[2]CEA, DAM, DIF, F-91297 Arpajon, France
[3]Université Bordeaux, CNRS, CENBG, UMR 5797, F-33170 Gradignan, France
[4]Université Paris-Saclay, CEA, LMCE, 91680 Bruyères-le-Châtel, France
[5]LPC Caen, ENSICAEN, Université de Caen, CNRS/IN2P3, F-Caen, France
[6]Lawrence Livermore National Laboratory, Livermore, California 94550, USA

February 19, 2021

February 19, 2021

Abstract

The National Nuclear Security Administration (NNSA)/DP French Alternative Energies and Atomic Energy Commission (CEA)/DAM agreement on cooperation on fundamental science is a U.S.-French collaborative effort to combine intellectual and experimental resources and further the relevant nuclear science. Recently, both the NNSA and CEA experimental teams performed high-statistics measurements of the ^{239}Pu(n,f) prompt fission neutron spectrum (PFNS) at the Los Alamos Neutron Science Center, both of which were recently published in the journal Physical Review C. These separate measurements used the same experimental area and a common neutron detector array, but differ in many aspects including background assessments, data acquisition systems and philosophies, fission detectors, and PFNS extraction techniques. Hence, some aspects of the experimental methods and associated uncertainties are highly correlated while others are independent. The results from both measurements broke new ground for PFNS measurements given their higher accuracy and more detailed study of corrections necessary for the measured quantity compared to existing literature measurements, and both will significantly impact PFNS nuclear data evaluations for the foreseeable future. The focus of this work is to document a comparison of the results from these distinct measurements in terms of the acquired data, the PFNS results, and the measured average PFNS energies. While systematic differences between the PFNS results are present on the 1–3% level, the acquired data relative to each respective measurement at low incident neutron energies are in remarkable agreement, as are the conclusions regarding the magnitude and position of features in the PFNS relating to second-chance fission, third-chance fission, and pre-equilibrium neutron emission.

Contents

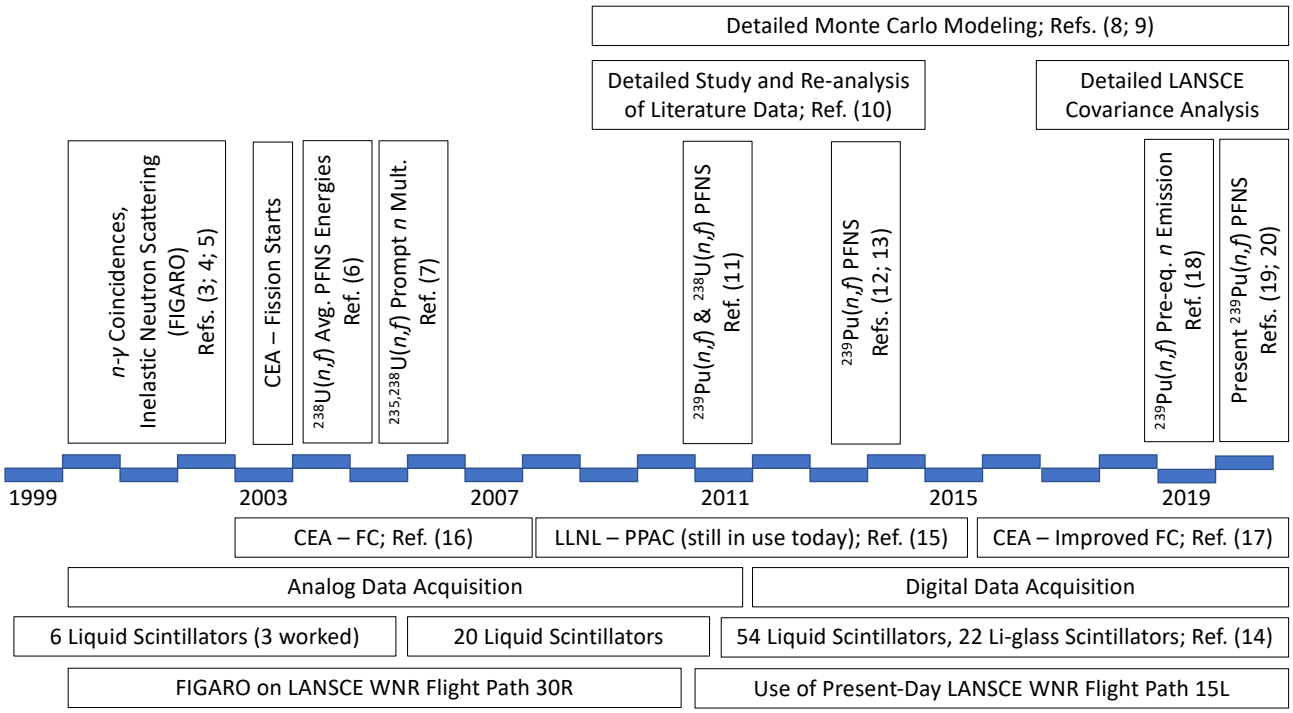

Figure 1: Timeline of development and collaboration between the NNSA and CEA starting from analog electronics and limited particle detection capabilities to modern, state-of-the-art experimental environments, leading to the efforts to measure the ^{239}Pu(n,f) PFNS compared in this work. See the text for a description.

1 Introduction to Fission Neutron Measurements at LANSCE and the Collaboration between the NNSA and CEA

Knowledge of fission physics, including the spectrum of prompt neutrons emitted from fission, termed the prompt fission neutron spectrum (PFNS), is essential for the description of systems driven by neutron-induced fission. Efforts to study nuclear fission predate the Manhattan Project, with the earliest PFNS evaluation report found in Los Alamos report LA-MS-1 from 1943 (1), and one of the most influential measurements of the average ^{239}Pu(n,f) prompt neutron multiplicity dating back to Fréhaut *et al.* in 1973 (2). With the purpose of advancing the collective understanding of the fission process and of the PFNS of major actinides, the National Nuclear Security Administration (NNSA)/DP French Alternative Energies and Atomic Energy Commission (CEA)/DAM agreement on cooperation on fundamental science was established nearly two decades ago.

The timeline of this collaboration with a selection of notable accomplishments is shown in Fig. 1, with experimental apparatus and equipment highlights shown on the lower part of this figure, and measurement and publication highlights shown in the upper portion. Initially, an array of six liquid scintillators was developed, though this was later increased to twenty detectors, and became known as the FIGARO array (3; 4; 5). Measurements of n-γ coincidences and inelastic neutron scattering were made with FIGARO, followed by fission measurements resulting in a collaborative publication in Physical Letters B on the ^{238}U average PFNS neutron energies (6), and another in Physical Review Letters on the ^{235}U and ^{238}U prompt neutron multiplicities (7).

An intensive look at previous experiments began over the years following this first measurement, resulting in detailed Monte Carlo simulations of what is now flight path 15L at the Weapons Neutron Research (WNR) facility, and of previous PFNS measurements. These simulations led to refinements of older experimental results, leading to the inflation of uncertainties on literature results in many cases based on a more modern understanding of the physical interactions of neutrons within the experimental environments, and a more accurate understanding of the nuclear physics involved in past measurements through steady improvements in the employed evaluated nuclear data libraries. This work also revealed significant errors in the analysis of these past experiments from which modern evaluations had been built (8; 9), and informed the description of needs for new ^{239}Pu(n,f) and ^{235}U(n,f) PFNS measurements (10) as well as the design of the detector arrays employed at WNR flight path 15L and of the flight

path itself. Approximately simultaneous with these efforts were collaborative measurements of the ^{235}U(n,f) and ^{239}Pu(n,f) PFNS later published in the journal Physical Review C based on data collected with the FIGARO array (11; 12; 13). Finally, the present-day experimental flight path was designed and built keeping in mind the pitfalls and systematic errors of past experiments.

In terms of experimental developments, work with the FIGARO detectors and simulation studies of past experiments guided significant advancements in neutron detector system. The "Chi-Nu" array of fifty-four liquid scintillator detectors was designed to measure a wider angular range of outgoing neutrons and cover a larger solid angle than the FIGARO array, and the Chi-Nu array of twenty-two Li-glass detectors was developed to be run in separate, complimentary measurements of lower outgoing neutron energies (14). It is a general characteristic of the PFNS from any fission event (spontaneous or neutron-induced) that a wide range of outgoing neutron energies, which introduces unique complications for PFNS measurements compared to, for example, neutron scattering where the emitted neutron energies are defined by kinematics. Thus, measuring the widest possible range of outgoing neutron energy is essential for a successful PFNS measurement.

In parallel with efforts on the neutron detection systems, both NNSA and CEA teams developed specialized fission detectors for PFNS measurements; the NNSA team developed a parallel-plate avalanche counter (PPAC) at Lawrence Livermore National Laboratory (LLNL) described in Ref. (15) still in use today, and the CEA team developed a fission chamber (FC) described in Ref. (16). The CEA FC was subsequently improved as described in Ref. (17) with additional improvements in associated frontend electronics to reduce data bias as well as reductions in structural mass to reduce neutron scattering. Both of these fission detectors were designed to minimize neutron scattering effects, which is especially important for materials near the source of fission neutrons, and also near the neutron detectors themselves.

Both the CEA and NNSA teams have performed measurements of the ^{239}Pu(n,f) PFNS at the present-day WNR flight path 15L, both of which were published shortly before the publication of this work (18; 19; 20). However, no direct comparisons of the results of these works were discussed in any previous publication. A direct comparison of these results is needed, as they are both being used in nuclear data evaluations of the ^{239}Pu(n,f) PFNS, and are guiding these evaluations across a large incident and outgoing energy range given the unparalleled high precision and broad energy coverage of the ^{239}Pu(n,f) PFNS from these measurements.

The purpose of this work is to provide a direct comparison of the results of the NNSA and CEA measurements of the ^{239}Pu(n,f) PFNS (19; 20). While the results of these measurements are correlated in many ways, they are separate results with distinct analysis philosophies and procedures. We describe the experimental area in Sec. 2, and the fission detectors, neutron detectors, and data acquisition systems in Sec. 3. The similarities and differences of each measurement are described as needed, with an effort to not repeat details provided in the respective publications from each experimental team (19; 20). In Sec. 4 we compare data analysis, PFNS extraction techniques, and uncertainty analysis of each measurement. Finally, a comparison of the results of the two experiments is provided in Sec. 5 with concluding remarks given in Sec. 6.

2 Experimental Measurement Area

Both measurements were carried out at the WNR facility at flight path 15L at the Los Alamos Neutron Science Center (LANSCE) (21; 22; 23). Incident neutrons were generated by proton spallation on a tungsten cylinder 21.5 m upstream of the target position. This distance was independently verified by both experimental teams through measurements of carbon resonances. Figure 2 shows some highlights of the experimental area design, including the notable presence of a "get-lost" basement beneath the experimental area. This pit is a 2 m deep recess of the the concrete subfloor with a thin aluminum panel making a false floor on which the neutron and fission detectors are placed. The neutron scattering effects from this aluminum floor are far reduced from that of the alternative concrete floor, and any neutrons that travel down through the thin aluminum floor beneath the detector array(s) necessarily have a total time of flight that is outside of the fission-neutron coincidence window of interest. The proton beam at WNR is pulsed with a spacing of approximately 1.8 μs between proton pulses, each of which is approximately 150 ps wide and is referred to as a micropulse. Groups of micropulses, 625 μs long, are delivered to WNR at a time-averaged rate of 100 s^{-1}. This beam structure is further described in Fig. 3. All details of the incident neutron beam and the experimental environment surrounding the employed detection systems were identical with the exception of beam intensity variations between experiments, and are described in both respective publications.

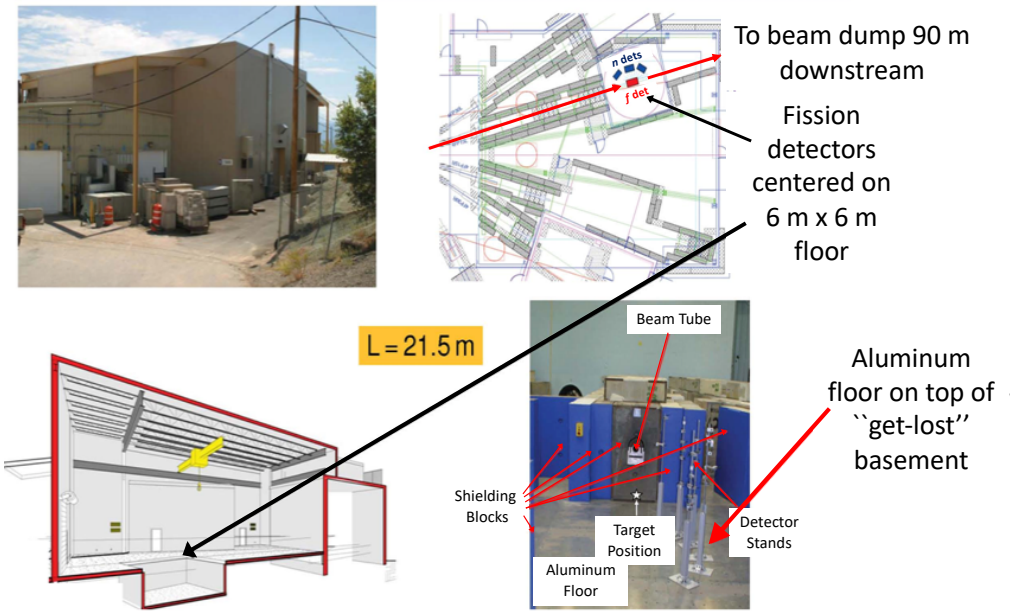

Figure 2: A series of figures showing WNR flight path 15L. Included here is an exterior view of the flight path building (upper left), a top-down schematic view of the WNR flight paths (upper right), and cutaway side view of the floor, walls, and ceiling of flight path 15L including a view of the "get-lost" basement (lower left), and a view of flight path 15L looking upstream towards the tungsten spallation target with reduced shielding and material in the experimental area (lower right).

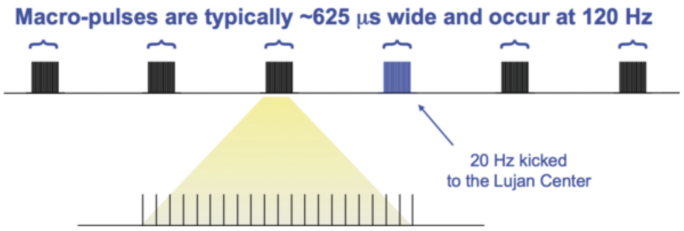

Figure 3: Shown here is an illustration of the WNR beam structure. Micropulses of protons approximately 150 ps wide are separated by approximately 1.8 μs from neighboring micropulses, and are bunched into macropulses. Macropulses are approximately 347 micropulses long, and are separated from neighboring macropulses by approximately 8.3 ms, with the exception of times when a macropulse is alternatively sent to the LANSCE Lujan center. This figure is a reproduction of Fig. 1 of Ref. (24).

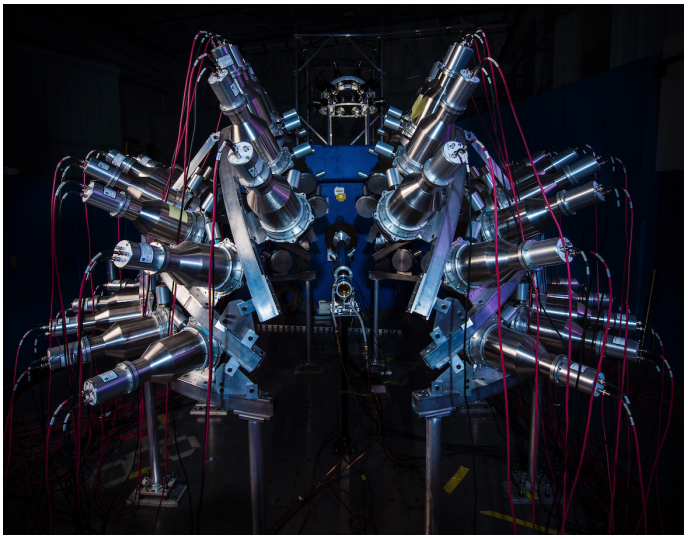

Figure 4: The fifty-four-detector liquid scintillator array used in both the NNSA and CEA experiments compared in this work is shown here. The NNSA fission detector is shown in the middle of the liquid scintillator array. The Li-glass detector array used by the NNSA experimental team is described in other publications (20; 24).

3 Fission Fragment and Neutron Detector Systems

Notable changes in experimental approach were present relating to fission and neutron detection methods. These details are described separately in Secs. 3.1 and 3.2, along with the data acquisition systems described in Sec. 3.3

3.1 Neutron Detectors

Both the CEA and NNSA teams used the same array of fifty-four EJ-309 (25) liquid scintillator detectors with Hamamatsu R1250A photomultiplier tubes (26), shown in Fig. 4 (14). The voltages applied to these detectors during data acquisition were roughly equal during both NNSA and CEA measurements, and were maintained within ± 0.5 V ($\approx 0.03\%$) during the course of each experiment. Consistent detector responses were also confirmed before and after both measurements using standard γ sources. The only notable difference in the experimental use of these detectors is that approximately 2.5 mm thick Pb shields were placed on the front of each liquid scintillator detector during the CEA measurement to reject low-energy γ rays to improve n-γ pulse-shape discrimination and extend it down to 200 keV. These shields were not included for the NNSA measurement to not increase neutron scattering effects.

One of the most significant differences between the NNSA and CEA measurements is the detection of low-energy neutrons from fission. In the CEA measurement, the response of the liquid scintillators was characterized down to outgoing neutron energies as low as 200 keV, allowing for a full reported PFNS energy range of 0.20 MeV to 10–12 MeV, depending on the incident energy bin. An extrapolation from 200 keV down to effectively 0 keV outgoing energy was performed using a Maxwellian functional form as described in Ref. (19). Conversely, in the NNSA measurement outgoing neutrons from 10 keV to 1.5 MeV were directly measured with a 22-detector Li-glass array in a separate, but correlated measurement. The Li-glass detectors are described in Refs. (20; 24). These Li-glass detectors measure low-energy neutrons via the ^{6}Li(n,t)α reaction, which lends itself well to low-energy neutron detection. The Li-glass measurement was then combined with the NNSA liquid scintillator measurement by first scaling each measurement to have the same area in the overlap region and then normalizing these scaled shapes together with proper covariance propagation, as recommended in Ref. (27) and described in Ref. (20), to report the PFNS from 10 keV to 10 MeV. It should be noted though that while the data from 10 keV to 100 keV are not shown in PFNS comparison plots in this work as there are no other measurements for direct comparison, they are available to be included in future nuclear data evaluations.

3.2 Fission Detectors

The fission fragment detection systems employed by each team are unique compared with each other. The NNSA team used a multiple-layer parallel-plate avalanche counter (PPAC) developed and fabricated by Lawrence Livermore National Laboratory as described in Ref. (15) with 100 mg total ^{239}Pu spread across twenty deposits. Further

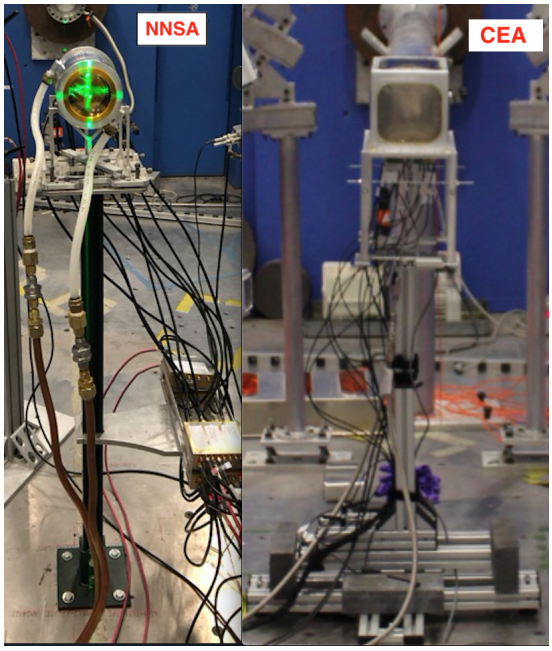

Figure 5: (color online) A side-by-side comparison of the fission detectors employed by both experimental teams. The NNSA PPAC is shown on the left panel, and the CEA FC is shown on the right. While the internal components of each fission detector can be seen in the respective published descriptions (15; 16; 17), the differences in structural and electronic configurations for each setup warrant documentation as they create different experimental environments.

improvements were made on the PPAC design in Ref. (15) for the NNSA measurements, including replacing G-10 fiberglass components to reduce neutron downscattering from hydrogenous materials and reversing the bias orientation to improve fission detection rates and separation of α particles from fission fragments. The CEA team used a multiple-layer fission ionization chamber (FC) designed by the CEA team as described in Ref. (17) with 47 mg total ^{239}Pu spread across 22 deposits. The FC described in Ref. (17) includes improvements implemented to the original FC design of Ref. (16), including a lower-mass housing, as well as dedicated pre-amplifiers that provide improved timing resolution and separation of fission fragments and α particles to reduce experimental bias. The NNSA PPAC operates at low pressure (typically 4.2 Torr), while the CEA FC operates at 75 Torr above the local atmospheric pressure of approximately 580 Torr at LANSCE.

The internal structure of each fission detector can be seen in the respective publications (15; 17). These fission detectors are compared side-by-side in Fig. 5, with the NNSA PPAC shown on the left panel, and the CEA FC shown on the right. Both chambers have sub-nanosecond resolution as measured from the γ-induced fission peak in the fission spectra, with the incident γ rays from the γ flash produced by incident protons reacting with the tungsten spallation target. The electronics, cables, gas lines, and structural materials relating to these fission detectors used during the separate measurements are shown as well to further document differences between the experimental configurations. The detection efficiency for the CEA FC is estimated to be approximately 95%, with 4% of fission events undetected if both fission fragments remain in the ^{239}Pu deposit and approximately 1% of fission fragments below the threshold for α particles. The NNSA PPAC is estimated to also detect approximately 95% of all fission fragments, though the fragment detection efficiency as a function of angle required careful Monte Carlo modeling efforts. Fission-fragment detection efficiencies and corrections for fission-fragment angular distributions are also discussed in the respective published works (19; 20).

3.3 Data Acquisition Systems and Random-Coincidence Backgrounds

Both measurement teams used digital data acquisition systems, though with different electronics. The CEA team employed 500 MHz, 12-bit Fast Acquisition System for Nuclear Research (FASTER) (28) digitizers, while the NNSA team used 500 MHz, 14-bit CAEN 1730B digitizers (29). Both configurations were effectively free of digital dead-time effects, and are further described in their respective citations. In terms of event recording, the CEA data acquisition system was synchronized on the fission signals, which then opened coincidence windows in which to collect coincident

neutron and t_0 (incident neutron time of flight start) signals. Conversely, the NNSA team recorded all t_0, outgoing neutron, and fission signals and integrals asynchronously, and performed coincidence analyses offline.

The details of the operation of each data acquisition system are also related to the method of determining random-coincidence backgrounds, i.e., accidental coincidences from fission and outgoing neutron signals that are not truly correlated to the same fission event despite falling within the same coincidence window. The CEA team measured the random-coincidence background associated with each incident neutron energy by introducing a random trigger to the data acquisition system, treated as a fission signal in this case. The NNSA team used the asynchronous t_0, fission, and outgoing neutron rates to determine the rate of random coincidences as described in Ref. (30). Both methods provide high-statistics measures of the random-coincidence background. While the techniques are different, this difference is not expected to be related to differences in the obtained results.

4 PFNS Extraction Techniques and Uncertainty Analysis

Once background-subtracted counts are obtained as a function of incident and outgoing neutron energy, the remaining tasks are to convert the measured data to a PFNS, and finalize the uncertainty analysis. The CEA PFNS results were extracted using efficiency measurements of spontaneous fission from a ^{252}Cf FC made to be as identical as possible to the ^{239}Pu FC. The NNSA team, on the other hand, relied on detailed Monte Carlo simulations to calculate an average correction to the measured data over a series of potential candidate reference spectra to convert the measured data to a PFNS. The details of these procedures are described in detail in their respective publications (19; 20), and are not repeated here. In principle these techniques result in some similar treatments of the experimental data in that the same procedure is applied to the data measured at each incident neutron energy, thereby correlating the results across incident neutron energy. However, the corrections to the data are different and may be a possible source of difference between the obtained results.

The uncertainty quantification approaches for results from both experiments also contain notable differences. Common to both experiments are studies of errors and biases from separation of fission fragments from α backgrounds in the respective fission fragment detectors, angular distributions of fission fragments, studies of fission neutron detection efficiency and scattering corrections, and low-energy incident neutron wraparound contamination. The CEA results are subject to systematic uncertainties in the efficiency and scattering corrections relating to the evaluated ^{252}Cf(sf) PFNS used for their analysis, yielding a 1:1 correlation of the measured results to the measured ^{252}Cf spectrum and the assumed ^{252}Cf PFNS, while the NNSA results are subject to systematic uncertainties from the use of Monte Carlo simulations, including partial correlations to the covariances associated with the relevant cross sections in the employed nuclear data library. One notable difference in the interpretation of the data from the CEA and NNSA measurements relates to differences in environmental neutron scattering effects between the measured ^{239}Pu(n,f) PFNS distributions at each incident energy and the reference spectra. In the CEA analysis this effect was investigated by Monte Carlo simulations and was seen to cause negligible error on the CEA results, believed to be the result of the low amount of structural material in the CEA FC housing. However, differences in neutron scattering for different PFNS distributions were determined to be a source of non-negligible systematic uncertainty across all measured incident neutron energies for the NNSA results for both the Li-glass and liquid scintillator measurements, also resulting from Monte Carlo simulations of the experimental environment. After normalization of the measured shape, this uncertainty for the NNSA measurement range from approximately 0.18–1.1% for the NNSA measurement in the range of 0.25–10 MeV outgoing neutron energy. Further details of these assessments can be found in the respective publications (19; 20).

The final uncertainties for the CEA result are contained within one-dimensional uncertainty trends for each incident energy, primarily resulting from statistical uncertainties, while the total uncertainties from the NNSA experiment were largely systematic and are contained within a single, 1300-by-1300 point covariance matrix correlating all measured PFNS data points at all incident energies. The reader is referred to Refs. (19; 20) for more details on the uncertainty analysis from each experiment. As a final note on nuclear data evaluations including the results from both experiments, these efforts are in progress and will be discussed in future publications. The complicated methods required to include both of these data sets in a nuclear data evaluation are outside the scope of this work.

5 Comparison of Experimental Results

Comparisons of the results of the NNSA and CEA measurements of the ^{239}Pu(n,f) PFNS are shown in this section, with identical analyses applied to each data set for each comparison. Figures 6, 7, 8, 9, 10, and 11 show PFNS comparisons for average incident neutron energies, $\langle E_n^{inc} \rangle$, near 1.5, 2.5, 4.5, 7.5, 10.5, and 13.5 MeV, respectively. All spectra are shown as a ratio to a 1.424 MeV Maxwellian distribution to eliminate the majority of the energy

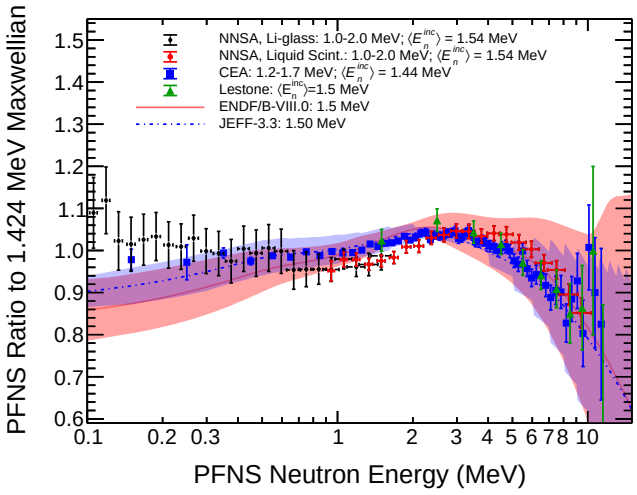

Figure 6: (color online) Shown here is a comparison of CEA (full, blue squares) (19) and NNSA (Li-glass data shown as full, black diamonds and liquid scintillator data shown as full, red circles) (20) PFNS results at $\langle E_n^{inc} \rangle \approx 1.5$ MeV. The exact $\langle E_n^{inc} \rangle$ values for each measurement are shown in the figure. Evaluations from ENDF/B-VIII.0 (31) and JEFF-3.3 (32) are shown for comparison (red and blue lines, respectively) alongside the data of Lestone and Shores (33), shown as the green triangles. All spectra are shown as a ratio to a 1.424 MeV Maxwellian distribution.

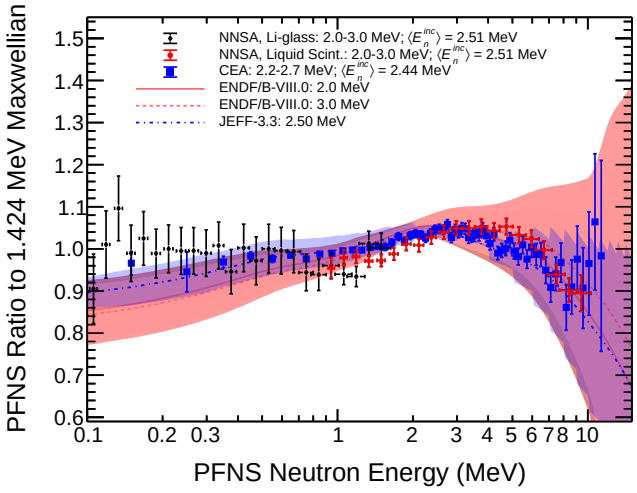

Figure 7: (color online) Shown here is a comparison of CEA (full, blue squares) (19) and NNSA (Li-glass data shown as full, black diamonds and liquid scintillator data shown as full, red circles) (20) PFNS results at $\langle E_n^{inc} \rangle \approx 2.5$ MeV. The exact $\langle E_n^{inc} \rangle$ values for each measurement are shown in the figure. Evaluations from ENDF/B-VIII.0 (31) and JEFF-3.3 (32) are shown for comparison as well. All spectra are shown as a ratio to a 1.424 MeV Maxwellian distribution.

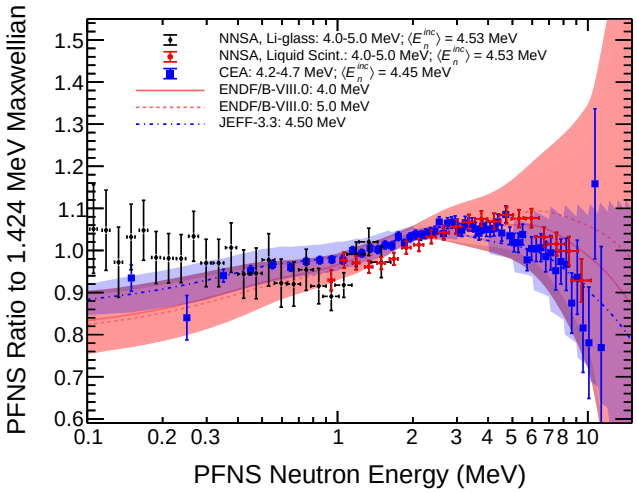

Figure 8: (color online) Shown here is a comparison of CEA (full, blue squares) (19) and NNSA (Li-glass data shown as full, black diamonds and liquid scintillator data shown as full, red circles) (20) PFNS results at $\langle E_n^{inc} \rangle \approx 4.5$ MeV. The exact $\langle E_n^{inc} \rangle$ values for each measurement are shown in the figure. Evaluations from ENDF/B-VIII.0 (31) and JEFF-3.3 (32) are shown for comparison as well. All spectra are shown as a ratio to a 1.424 MeV Maxwellian distribution.

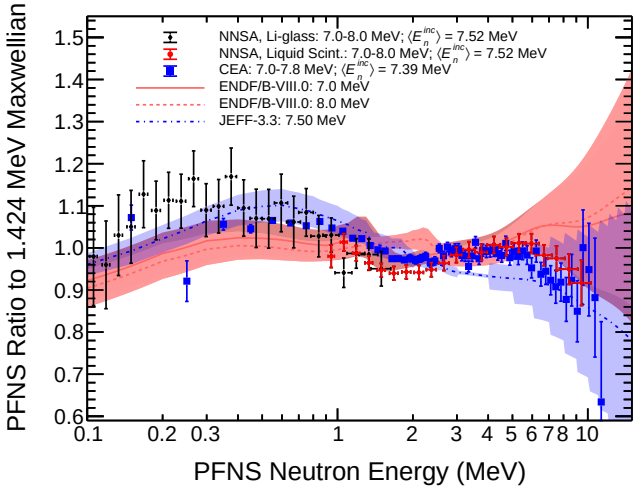

Figure 9: (color online) Shown here is a comparison of CEA (full, blue squares) (19) and NNSA (Li-glass data shown as full, black diamonds and liquid scintillator data shown as full, red circles) (20) PFNS results at $\langle E_n^{inc} \rangle \approx 7.5$ MeV. The exact $\langle E_n^{inc} \rangle$ values for each measurement are shown in the figure. Evaluations from ENDF/B-VIII.0 (31) and JEFF-3.3 (32) are shown for comparison as well. All spectra are shown as a ratio to a 1.424 MeV Maxwellian distribution.

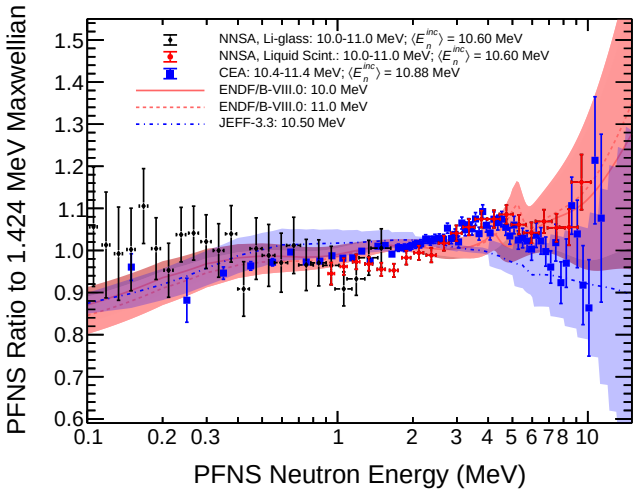

Figure 10: (color online) Shown here is a comparison of CEA (full, blue squares) (19) and NNSA (Li-glass data shown as full, black diamonds and liquid scintillator data shown as full, red circles) (20) PFNS results at $\langle E_n^{inc} \rangle \approx 10.5$ MeV. The exact $\langle E_n^{inc} \rangle$ values for each measurement are shown in the figure. Evaluations from ENDF/B-VIII.0 (31) and JEFF-3.3 (32) are shown for comparison as well. All spectra are shown as a ratio to a 1.424 MeV Maxwellian distribution.

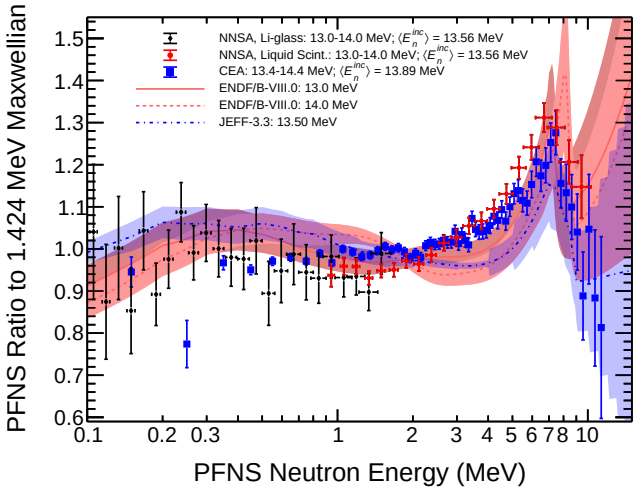

Figure 11: (color online) Shown here is a comparison of CEA (full, blue squares) (19) and NNSA (Li-glass data shown as full, black diamonds and liquid scintillator data shown as full, red circles) (20) PFNS results at $\langle E_n^{inc} \rangle \approx 13.5$ MeV. The exact $\langle E_n^{inc} \rangle$ values for each measurement are shown in the figure. Evaluations from ENDF/B-VIII.0 (31) and JEFF-3.3 (32) are shown for comparison as well. All spectra are shown as a ratio to a 1.424 MeV Maxwellian distribution.

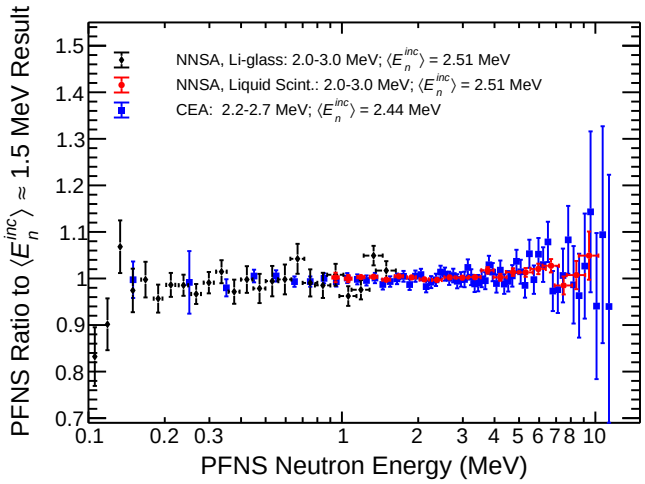

Figure 12: (color online) Shown here is a comparison of CEA (full, blue squares) and NNSA (Li-glass data shown as full, black diamonds and liquid scintillator data shown as full, red circles) PFNS results at at $\langle E_n^{inc} \rangle \approx 2.5$ MeV shown as a ratio to the result at $\langle E_n^{inc} \rangle \approx 1.5$ MeV for each measurement.

dependence of the PFNS as a function of outgoing neutron energy, and focus on finer details of the PFNS shapes. The CEA measurements are shown in blue, while the NNSA measurements with the liquid scintillators detector are shown in red, and NNSA Li-glass measurements in black. Note that the CEA data points at 150 keV outgoing neutron energy are extrapolated by fitting the low-energy portion of the measured shape with a Maxwellian distribution, and are not directly measured. This procedure is described in more detail in Ref. (19). Relevant ENDF/B-VIII.0 (31) and JEFF-3.3 (32) evaluations are shown as well with shaded regions displaying the 1-σ uncertainties from these evaluations. Experimental data are scaled such that they have the same area over the plotted outgoing energy range as the lowest incident energy ENDF/B-VIII.0 trend on each figure. It should also be emphasized that the results from each measurement are not identically binned in incident or outgoing neutron energy. For example, the average incident neutron energy of the NNSA measurement in Fig. 6 is 1.54 MeV, while the average incident neutron energy for the CEA data in the same figure is 1.44 MeV. Therefore, direct comparisons of the experimental results must consider these changes in incident energy, which can produce small shape changes in the reported results.

The results of these separate measurement campaigns are in remarkably close agreement, with the majority of differences only on the 1–3% level, with these small disagreements primarily appearing in the 0.7–2 MeV and 5–8 MeV outgoing neutron energy ranges of the PFNS. It is also relevant to compare both data sets to the data of Lestone and Shores (33) in Fig. 6 as these data have shown to be have a significant impact on nuclear data evaluations (10). Both the NNSA and CEA data sets generally agree with Lestone and Shores in Fig. 6, though the shape of the CEA result appears to agree better overall with Ref. (33). Additionally, these two measurements agree well on the presence and magnitude of the features apparent in the PFNS as second-chance fission becomes available, seen as the increase in relative PFNS contribution from 0.1–1.0 MeV in Fig. 9. Perhaps the most notable conclusion from each work is that third-chance fission features, seen as an excess in the ENDF/B-VIII.0 and JEFF-3.3 evaluated PFNS distributions from outgoing neutron energies of 0.3–1.5 MeV, are not present in either PFNS measurement to nearly the extent predicted by the plotted evaluations, as demonstrated by the clear shape differences between data and evaluations in Fig. 11. Both teams have also clearly measured a component of the ^{239}Pu(n,f) PFNS resembling a peak as seen at the higher outgoing energies in Figs. 10 and 11. It was suggested in Ref. (18) that this feature is the pre-equilibrium component of the PFNS as it appears to match predictions of this PFNS component given in Refs. (34; 35; 36; 37). Despite the overall good agreement between these results, there is a shape difference between the results from the NNSA and CEA teams, and that shape difference appears to be largely consistent across incident neutron energy.

In an attempt to identify the source of differences between these data sets, we can take advantage of the similar overlapping coverage in incident and outgoing neutron energies. Instead of comparing results as a ratio to a Maxwellian, we study results as a ratio to each respective PFNS result near the lowest common average incident energy, $\langle E_n^{inc} \rangle \approx 1.5$ MeV here. Displaying the results from each experiment as a ratio in this way cancels aspects of data analysis and PFNS extraction that are consistent across incident energy, primarily the different methods of correcting the data for detector response, scattering, and efficiencies. While the background methods employed by each team are consistently applied across incident energy leading one to potentially assume that the different background techniques

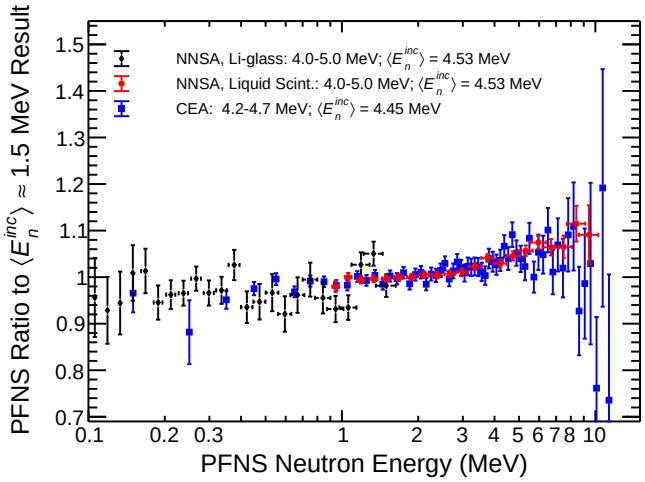

Figure 13: (color online) Shown here is a comparison of CEA (full, blue squares) and NNSA (Li-glass data shown as full, black diamonds and liquid scintillator data shown as full, red circles) PFNS results at at $\langle E_n^{inc} \rangle \approx 4.5$ MeV shown as a ratio to the result at $\langle E_n^{inc} \rangle \approx 1.5$ MeV for each measurement.

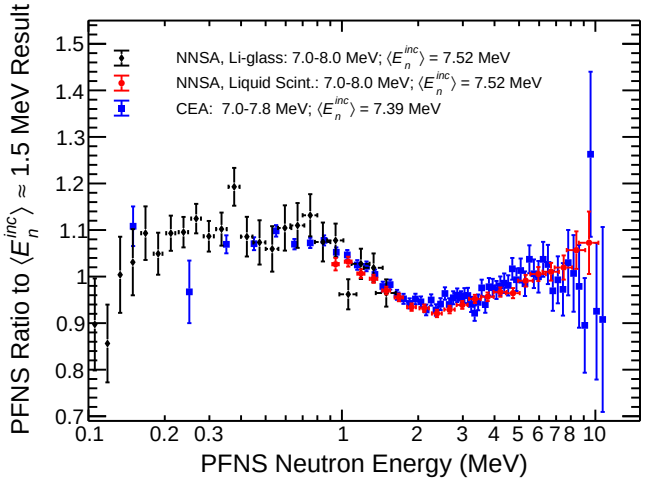

Figure 14: (color online) Shown here is a comparison of CEA (full, blue squares) and NNSA (Li-glass data shown as full, black diamonds and liquid scintillator data shown as full, red circles) PFNS results at at $\langle E_n^{inc} \rangle \approx 7.5$ MeV shown as a ratio to the result at $\langle E_n^{inc} \rangle \approx 1.5$ MeV for each measurement.

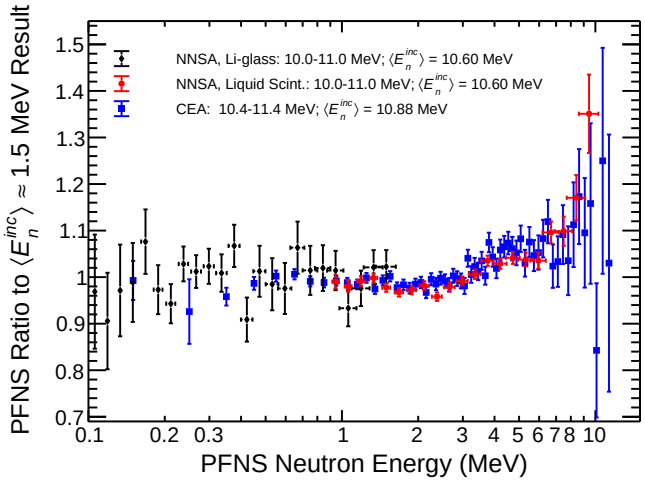

Figure 15: (color online) Shown here is a comparison of CEA (full, blue squares) and NNSA (Li-glass data shown as full, black diamonds and liquid scintillator data shown as full, red circles) PFNS results at at $\langle E_n^{inc} \rangle \approx 10.5$ MeV shown as a ratio to the result at $\langle E_n^{inc} \rangle \approx 1.5$ MeV for each measurement.

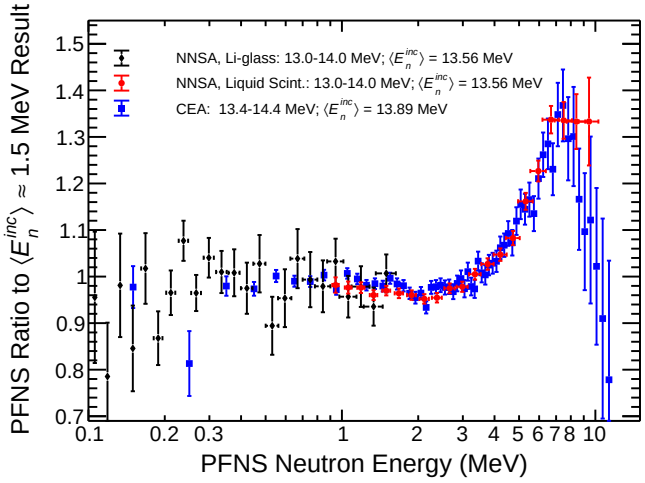

Figure 16: (color online) Shown here is a comparison of CEA (full, blue squares) and NNSA (Li-glass data shown as full, black diamonds and liquid scintillator data shown as full, red circles) PFNS results at at $\langle E_n^{inc} \rangle \approx 13.5$ MeV shown as a ratio to the result at $\langle E_n^{inc} \rangle \approx 1.5$ MeV for each measurement.

employed by each team cancel in this kind of comparison, the backgrounds at each incident energy range are different and are already subtracted from the measured data. Therefore, aspects of background measurement and subtraction for each data set do not cancel for these comparisons. Furthermore, the threshold placed between α particles and fission fragments in the fission detector spectra from each experiment introduces a bias to the data, as it places a cut on the measured mass, charge, total kinetic energy, and angular distributions of the emitted fission fragments. The capability of a fission detector to separate α and fission fragments is crucial to reduce this bias. As fission fragment properties change with incident energy, the bias on these distributions may change as well. Moreover, the NNSA PPAC and the CEA FC do not behave identically, implying that the data bias is not the same. The emitted neutron energy spectra are correlated to these fission fragment properties, and therefore the biases do not in principle cancel in these PFNS ratio comparisons. However, when fission fragment properties are similar, e.g., for nearby or neighboring incident energy ranges, the biases are likely similar and partially compensate each other. Therefore, only part of the data bias at each incident energy remains in these ratios, with the amount depending on the experiment, along with differences in experimental environment details and data acquisition methods, among others. Thus, this kind of manipulation of the data allows for a more direct comparison of the acquired data (i.e., neutron counts coincident with fission and above the determined background) instead of a convolution of the acquired data with other corrections intended to convert the data to a PFNS.

Figures 12, 13, 14, 15, and 16 compare the results as a ratio to the $\langle E_n^{inc} \rangle \approx 1.5$ MeV results of each measurement for $\langle E_n^{inc} \rangle \approx 2.5$, 4.5, 7.5, 10.5, and 13.5 MeV, respectively. For the NNSA results, the covariances were propagated through to the data shown in these figures, which reduces the impact of uncertainties that are correlated across incident neutron energy. For the CEA data, systematic uncertainties relating to the use of the ^{252}Cf(sf) PFNS as a reference were excluded from these ratios as they are constant across incident energy. It should be noted that the differences in binning of the incident and outgoing neutron energies, with NNSA measurements typically choosing to report wider bins for both energies, impact the statistical uncertainties observed in each data point. This should be considered when comparing uncertainties on the these and all comparison figures in this work.

In Fig. 12, the observed data are not significantly different than those observed at $\langle E_n^{inc} \rangle \approx 1.5$ MeV, so minimal change is expected and this figure serves as a benchmark for the comparisons at higher incident energies. Going slightly higher to $\langle E_n^{inc} \rangle \approx 4.5$ MeV, the PFNS is weighted towards higher outgoing neutron energies with both NNSA and CEA results agreeing well for all outgoing energies. Next, at $\langle E_n^{inc} \rangle \approx 7.5$ MeV, the data from each experiment again agree very well, implying that the shape and magnitude of the second-chance fission features observed in the data are nearly identical. Finally, the peak features seen in Figs. 15 and 16, potentially relating to pre-equilibrium neutron emission, appear to again be in excellent agreement between the two data sets, indicating consistency with respect to this feature as well. While the results from each team relative to their respective $\langle E_n^{inc} \rangle \approx 1.5$ MeV results are not perfectly identical, the general agreement between the results shown in this form may support, but does not necessarily prove, the possibility of the PFNS extraction methods being responsible for the differences in the reported PFNS results. The agreement of the results in Figs. 12–16 is also consistent with the possible presence of one or more unidentified sources of error in the acquired data common between these correlated experiments, generally termed unrecognized sources of uncertainties (USU) (38), though such issues are difficult to identify by definition.

The conclusions made regarding shape of the PFNS results are also reflected in the mean energies of the PFNS, $\langle E \rangle$, shown in the top panel of Fig. 17 for an integrated outgoing neutron energy range of 0.01-10.0 MeV. These average energies were calculated over the same outgoing neutron energy range for each data set, including the extrapolated data for the CEA measurements below 200 keV. Relative uncertainty trends are shown in the bottom panel of Fig. 17. While in most cases there is a slight shift in the average energy of up to approximately 10 keV ($\approx$0.5% of $\langle E \rangle$), the shapes of the $\langle E \rangle$ trends are very similar. The most notable similarities are the slopes from $E_n^{inc} = 1$–5 MeV implying a similar extrapolation to thermal incident neutron energies, a similar position and magnitude of a drop in $\langle E \rangle$ at the second-chance fission threshold from 6–8 MeV incident neutron energy, and only a minor feature in $\langle E \rangle$ from third-chance fission from 13–16 MeV incident neutron energy.

Many of these details of PFNS changes as a function of incident neutron energy are not reproduced well by any particular evaluation. Thus both of these measurements will provide vital guidance to future ^{239}Pu(n,f) PFNS evaluations and model calculations, specifically the position and magnitude of the drops in $\langle E \rangle$ at multi-chance fission thresholds as they relate almost directly to the fission barrier heights and relevant level densities. The uncertainties on $\langle E \rangle$ at $E_n^{inc} \approx 1.5$ MeV from these measurements of approximately 25.7 keV for the total uncertainty of the NNSA measurement and 5.3 keV for the CEA measurement are to be compared to the uncertainties of 37 keV for ENDF/B-VIII.0 (31) (which is identical to the CIELO (39) result) and 93 keV for JEFF-3.3 (32) at approximately the same incident neutron energy. However, these evaluated uncertainties correspond to $\langle E \rangle$ values calculated over the entire outgoing neutron energy range of the PFNS as opposed to the $E_n^{out} = 0.01$-10.0 MeV range used for the experimental results here. Despite the differences in integration range for these uncertainties, the NNSA and CEA measurements

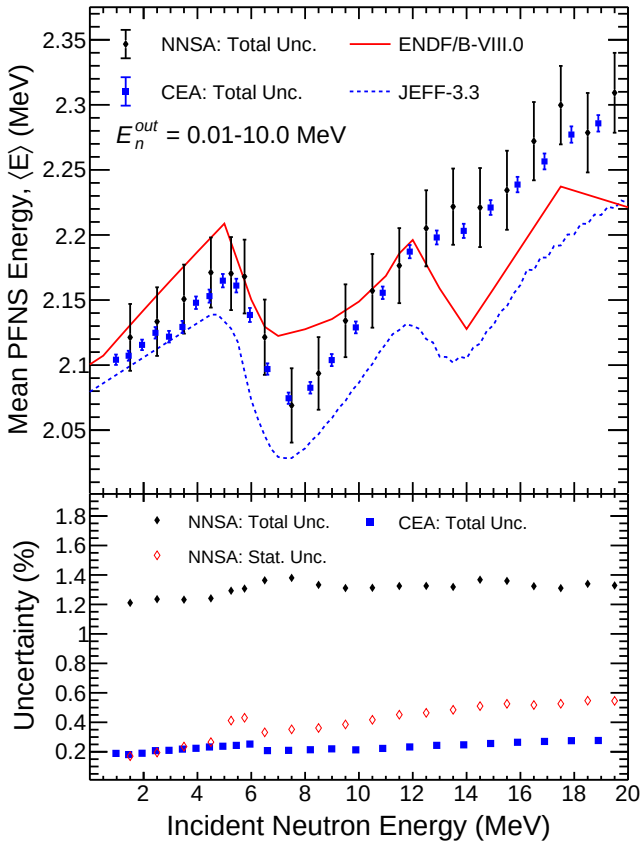

Figure 17: (color online) A comparison of average PFNS neutron energies, $\langle E \rangle$, as a function of incident neutron energy are shown in the top panel, with uncertainty trends shown in the bottom panel. Total uncertainties for the CEA results are shown as the full, blue squares, while total uncertainties for the NNSA results are shown as the full, black diamonds in both top and bottom panels. Statistical uncertainties for the NNSA results are shown as the open, red diamonds in the bottom panel. Evaluation results from ENDF/B-VIII.0 (31) and JEFF-3.3 (32) are shown as the solid red and blue dashed, respectively. All $\langle E \rangle$ results are integrated over 0.01–10 MeV PFNS energies, including evaluations shown here.

will yield higher precision on mean energies for future evaluations.

6 Conclusions

The collaborative measurements of the ^{239}Pu(n,f) PFNS by the NNSA and CEA experimental teams involved different approaches to experimental design and data analysis techniques. The teams applied independent data acquisition electronics, data event recording and coincidence detection algorithms, random-coincidence background calculation techniques, fission detectors, and PFNS extraction techniques. While these measurements are internally correlated through the use of the same liquid scintillator detector array, incident neutron beam, and experimental measurement area, the differences in these approaches to PFNS measurement yield separate and complimentary results that are excellent tests of each methodology.

PFNS results from these two measurements are generally in agreement for all incident and outgoing neutron energies. This agreement includes estimates of extrapolation of mean PFNS energy to thermal incident neutron energies, shape of second-chance fission features, the overall lack of third-chance fission features, and the clear presence of the a peak-like feature in the PFNS potentially relating to the pre-equilibrium component of the PFNS. Small shape differences on the order of 1–3% are present within these results that also appear to be relatively constant as a function of incident neutron energy, and this systematic change between the data sets is also reflected in the average energy comparison. The source of discrepancy was also investigated by comparing results as a ratio to the $\langle E_n^{inc} \rangle \approx 1.5$ MeV PFNS of each respective data set. This comparison yielded excellent agreement between the two experiments, much better than between the PFNS results themselves. This improved agreement demonstrated that the data obtained from each experiment after application of each separate data processing method, fission detector, and background subtraction technique, but before corrections for detector efficiencies and neutron scattering effects are very similar. This could imply that the differences between the results primarily lie in the different approaches to neutron scattering and efficiency corrections. However, we note that a caveat to this agreement is the partial presence of data bias effects in these PFNS ratios resulting from the partial compensation of effects from any similarities in fission fragment properties at the different incident neutron energy ranges. Thus, the fission detector performance could also partially relate to the small disagreements observed in the PFNS results themselves. Both experimental teams are also pursuing measurement and analysis of the PFNS from other actinides in similar experiments, and an analogous comparative analysis of these results will likely follow. These new measurements and comparisons may provide guidance as to the source of the small disagreements seen between the results of each experimental team.

Despite any differences in the approaches of each experimental team, the ability to compare two measurements of the ^{239}Pu(n,f) PFNS on the percent-difference level, when previous literature measurements of the ^{239}Pu(n,f) PFNS did not measure nearly the high precision or wide range of incident and outgoing energies obtained in both of these works, gives added confidence to the results of the collaboration. This level of precision and agreement between the results of the two experimental efforts will make the CEA and NNSA measurements of the ^{239}Pu(n,f) PFNS the dominant source of experimental input for the relevant nuclear data evaluations for the foreseeable future.

7 Acknowledgements

The results discussed in this work benefited from the use of the LANSCE accelerator facility. This work was performed under the auspices of the U.S. Department of Energy by Los Alamos National Laboratory, by Lawrence Livermore National Security, LLC under contract DE-AC52-07NA27344, and under the NNSA/DP CEA/DAM agreement on cooperation on fundamental science. Los Alamos National Laboratory is operated by Triad National Security, LLC, for the National Nuclear Security Administration of the U.S. Department of Energy (Contract No. 89233218CNA000001).

References

[1] W. E. Bennett and H. T. Richards, "A Discussion of the Fission Neutron Spectrum," *LA-MS-1*, 1943.

[2] J. Fréhaut, G. Mosinski, and M. Soleilhac, "Recent Results in ν Measurements Between 1.5 and 15 MeV," *EANDC Topical Conference*, vol. 154, p. 67, 1973 (EXFOR Entry 204900).

[3] R. C. Haight, J. M. O'Donnell, L. Zanini, M. Devlin, and D. Rochman, "FIGARO: Measuring Neutron Emission Spectra with a White Neutron Source," *LA-UR-02-5486*, 2002.

[4] D. Rochman, R. C. Haight, J. M. O'Donnell, M. Devlin, T. Ethvignot, and T. Granier, "Neutron-Induced Reaction Studies at FIGARO using a Spallation Source," *Nucl. Instrum. Methods A*, vol. 523, p. 102, 2004.

[5] D. Rochman, R. C. Haight, J. M. O'Donnell, M. Devlin, T. Ethvignot, *et al.*, "Neutron Emission Spectra from Inelastic Scattering on ^{58,60}Ni with a White Neutron Source at FIGARO," *AIP Conf. Proc.*, vol. 769, p. 985, 2005.

[6] T. Ethvignot, M. Devlin, R. Drosg, T. Granier, R. C. Haight, *et al.*, "Prompt-fission-neutron Average Energy for ^{238}U from threshold to 200 MeV," *Phys. Lett. B*, vol. 575, p. 221, 2003.

[7] T. Ethvignot, M. Devlin, H. Duarte, T. Granier, R. C. Haight, *et al.*, "Neutron Multiplicity in the Fission of ^{238}U and ^{235}U with Neutrons up to 200 MeV," *Phys. Rev. Lett.*, vol. 94, p. 052701, 2005.

[8] T. N. Taddeucci, R. C. Haight, H. Y. Lee, D. Neudecker, J. M. O'Donnell, *et al.*, "Multiple-scattering Corrections to Measurements of the Prompt Fission Neutron Spectrum," *Nucl. Data Sheets*, vol. 123, p. 135, 2015.

[9] D. Neudecker, R. Capote, D. L. Smith, and T. Burr, "Impact of the Normalization Condition and Model Information on Evaluated Prompt Fission Neutron Spectra and Associated Uncertainties," *Nucl. Sci. Eng.*, vol. 179, p. 381, 2015.

[10] D. Neudecker, T. N. Taddeucci, R. C. Haight, H. Y. Lee, M. C. White, *et al.*, "The Need for Precise and Well-documented Experimental Data on Prompt Fission Neutron Spectra from Neutron-induced Fission of ^{239}Pu," *Nucl. Data Sheets*, vol. 131, p. 289, 2016.

[11] S. Noda, R. C. Haight, R. O. Nelson, M. Devlin, J. M. O'Donnell, *et al.*, "Prompt Fission Neutron Spectra from Fission Induced by 1 to 8 MeV Neutrons on ^{235}U and ^{239}Pu using the Double Time-of-Flight Technique," *Phys. Rev. C*, vol. 83, p. 034604, 2011.

[12] A. Chatillon, G. Bélier, T. Granier, B. Laurent, B. Morillon, *et al.*, "Measurement of the Prompt Neutron Spectra from the ^{239}Pu(n,f) Fission Reaction for Incident Neutron Energies from 1 to 200 MeV," *Phys. Rev. C*, vol. 89, p. 014611, 2014.

[13] T. Granier, "Reanlysis of ^{239}Pu Prompt Fission Neutron Spectra," *Phys. Proc.*, vol. 64, p. 183, 2015.

[14] R. C. Haight, H. Y. Lee, T. N. Taddeucci, J. M. O'Donnell, B. A. Perdue, *et al.*, "The Prompt Fission Neutron Spectrum (PFNS) Measurement Program at LANSCE," *Nucl. Data Sheets*, vol. 119, p. 205, 2014.

[15] C. Y. Wu, R. A. Henderson, R. C. Haight, H. Y. Lee, T. N. Taddeucci, *et al.*, "A Multiple Parallel-plate Avalanche Counter for Fission-Fragment Detection," *Nucl. Instrum. and Methods A*, vol. 794, p. 76, 2015.

[16] J. Taieb, B. Laurent, G. Bélier, A. Sardet, and C. Varignon, "A New Fission Chamber Dedicated to Prompt Fission Neutron Spectra Measurements," *Nucl. Instrum. and Methods A*, vol. 833, p. 1, 2016.

[17] B. Laurent, J. Taieb, G. Bélier, P. Marini, and P. Morfouace, "New Developments of a Fission Chamber for Very High Radioactivity Samples," *Nucl. Instrum. and Methods A*, vol. 990, p. 164966, 2021.

[18] K. J. Kelly, T. Kawano, J. M. O'Donnell, J. A. Gomez, M. Devlin, *et al.*, "Pre-Equilibrium Asymmetries in the ^{239}Pu(n,f) Prompt Fission Neutron Spectrum," *Phys. Rev. Lett.*, vol. 122, p. 072503, 2019.

[19] P. Marini, J. Taieb, B. Laurent, G. Belier, A. Chatillon, *et al.*, "Prompt Fission Neutrons in the ^{239}Pu(n,f) Reaction," *Phys. Rev. C*, vol. 101, p. 044614, 2020.

[20] K. J. Kelly, M. Devlin, J. M. O'Donnell, J. A. Gomez, D. Neudecker, *et al.*, "Measurement of the ^{239}Pu(n,f) Prompt Fission Neutron Spectrum from 10 keV to 10 MeV Induced by Neutrons of energy 1–20 MeV," *Phys. Rev. C*, vol. 102, p. 034615, 2020.

[21] S. A. Wender, S. J. Seestrom-Morris, and R. O. Nelson, "A White Neutron Source from 1 to 400 MeV," *J. Phys. G: Nucl. Phys.*, vol. 14, p. S417, 1988.

[22] P. W. Lisowski, C. D. Bowman, G. J. Russell, and S. A. Wender, "The Los Alamos National Laboratory Spallation Neutron Sources," *Nucl. Sci. Eng.*, vol. 106, p. 208, 1990.

[23] P. W. Lisowski and K. F. Schoenberg, "The Los Alamos Neutron Science Center," *Nucl. Instrum. Methods A*, vol. 562, p. 910, 2006.

[24] M. Devlin, J. A. Gomez, K. J. Kelly, R. C. Haight, J. M. O'Donnell, *et al.*, "The Prompt Fission Neutron Spectrum of ^{235}U(n,f) below 2.5 MeV for Incident Neutrons from 0.7 to 20 MeV," *Nucl. Data Sheets*, vol. 148, p. 322, 2018.

[25] https://eljentechnology.com/products/liquid-scintillators/ej-301-ej-309.

[26] https://www.hamamatsu.com.

[27] K. J. Kelly, J. M. O'Donnell, D. Neudecker, M. Devlin, and J. A. Gomez, "The Analysis of Shape Data Including Normalization and the Impact on Prompt Fission Neutron Spectrum Measurements," *Nucl. Instrum. and Methods A*, vol. 943, p. 162449, 2019.

[28] FASTER, LPC-Caen, http://faster.in2p3.fr (2013).

[29] https://www.caen.it/products/v1730.

[30] J. M. O'Donnell, "A New Method to Reduce the Statistical and Systematic Uncertainty of Chance Coincidence Backgrounds Measured with Waveform Digitizers," *Nucl. Instrum. Methods A*, vol. 805, p. 87, 2016.

[31] D. A. Brown, M. B. Chadwick, R. Capote, A. C. Kahler, A. Trkov, *et al.*, "ENDF/B-VIII.0: The 8^{th} Major Release of the Nuclear Reaction Data Library with CIELO-project Cross Sections, New Standards, and Thermal Scattering Data," *Nucl. Data Sheets*, vol. 148, p. 1, 2018.

[32] A. J. Plompen, O. Cabellos, C. De Saint Jean, M. Fleming, A. Algora, *et al.*, "The Joint Evaluated Fission and Fusion Nuclear Data Library, JEFF-3.3," *Eur. Phys. J.*, vol. 56, p. 181, 2020.

[33] J. P. Lestone and E. F. Shores, "Uranium and Plutonium Average Prompt-Fission Neutron Energy Spectra (PFNS) from the Analysis of NTS NUEX Data," *Nucl. Data Sheets*, vol. 119, p. 213, 2014.

[34] E. Gadioli and P. E. Hodgson, *Pre-equilibrium Nuclear Reactions*. Oxford University Press, New York, 1992.

[35] T. Kawano, T. Ohsawa, M. Baba, and T. Nakagawa, "Effect of the Pre-equilibrium Process upon Fast Neutron Fission Spectra from ^{238}U," *Phys. Rev. C*, vol. 63, p. 034601, 2001.

[36] A. Tudora, B. Morillon, F.-J. Hambsch, G. Vladuca, and S. Oberstedt, "A Refined Model for ^{235}U(n,f) Prompt Fission Neutron Multiplicity and Spectrum Calculation with Validation in Integral Benchmarks," *Nucl. Phys*, vol. A756, p. 176, 2005.

[37] R. Capote, Y.-J. Chen, F.-J. Hambsch, N. V. Kornilov, J. P. Lestone, *et al.*, "Prompt Fission Neutron Spectra of Actinides," *Nucl. Data Sheets*, vol. 131, p. 1, 2016.

[38] R. Capote, S. Badikov, A. D. Carlson, I. Duran, F. Gunsing, *et al.*, "Unrecognized Sources of Uncertainties (USU) in Experimental Nuclear Data," *Nucl. Data Sheets*, vol. 163, p. 191, 2020.

[39] M. B. Chadwick, R. Capote, A. Trkov, M. W. Herman, D. A. Brown, *et al.*, "CIELO Collaboration Summary Results: International Evaluations of Neutron Reactions on Uranium, Plutonium, Iron, Oxygen and Hydrogen," *Nucl. Data Sheets*, vol. 148, p. 189, 2018.